CORE
Metadata, citation and similar papers at core.ac.uk
Provided by Xiamen University Institutional Repository

Journal of Alloys and Compounds 818 (2020) 152911

Contents lists available at ScienceDirect

Journal of Alloys and Compounds

journal homepage: http://www.elsevier.com/locate/jalcom

Rational design of interlaced Co_9S_8/carbon composites from ZIF-67/cellulose nanofibers for enhanced lithium storage

Shihang Guo [a], Pengcheng Zhang [a], Yi Feng [a, **], Zhongguo Wang [a], Xiaodan Li [b], Jianfeng Yao [a, *]

[a] College of Chemical Engineering, Jiangsu Key Lab for the Chemistry & Utilization of Agricultural and Forest Biomass, Nanjing Forestry University, Nanjing, 210037, China
[b] School of Materials Science and Engineering, Xiamen University of Technology, Xiamen, 361024, China

ARTICLE INFO

Article history:
Received 30 July 2019
Received in revised form
26 October 2019
Accepted 3 November 2019
Available online 5 November 2019

Keywords:
Co_9S_8
Cellulose nanofibers
ZIF-67
Li-ion batteries anode

ABSTRACT

Cellulose nanofibers (CNFs) are used to string ZIF-67 particles and interlaced Co_9S_8/porous carbon composite (Co_9S_8/C-CNFs) is obtained via carbonization and sulphidation of ZIF-67/CNFs composites. The CNFs can effectively limit the growth of ZIF-67 particles and avoid the agglomeration and most importantly, serve as the conductive skeleton to "bridge" carbonized ZIF-67 particles after carbonization. Due to the unique structure and the improved conductivity, Co_9S_8/C-CNFs as anode of lithium-ion batteries exhibits enhanced electrochemical properties and the specific capacity is 700 mAh g^{-1} at current density of 500 mA g^{-1} after 150 cycles compared to that of 342 mAh g^{-1} for samples without CNFs incorporation. Such nanoscale design may boost to explore other nanocomposites for energy storage.
© 2019 Elsevier B.V. All rights reserved.

1. Introduction

Nowadays, lithium-ion batteries (LIBs) have brought wireless revolution for cell phones, laptop computers and digital cameras [1]. However, Due to the relatively low specific capacity of commercial graphite anode, it was unable to meet the demands of high-performance next-generation LIBs. As a result, it is urgent to develop anode materials with higher energy density and longer cycling life [2]. To this end, transition metal sulfides have showed great potential as the anode materials for LIBs because of their high theoretical specific capacities and excellent electrochemical activities [3,4]. Unfortunately, the severe volume expansion and low electrical conductivity of sulfides stand in the way of their practical applications. To solve these problems, tremendous efforts have been devoted. In these methods, wrapping with carbon materials has been effective for fast charge transfer kinetics and alleviating volume expansion [5,6]. One-dimension (1D) carbon materials have displayed desirable and fascinating electrochemical properties due to the excellent mechanical properties and good oriented electronic/ionic transport pathway [7,8]. For example, carbon nanotubes [9] and carbon nanofibers [10] have been used to wrap metal sulfides and such wrapping showed enormous advantages. Therefore, it is promising to develop metal sulfides/1D carbonaceous material nanocomposites as potential high-performance anodes for LIBs. So far, the choice of 1D carbon nanofiber are mainly carbon nanotubes and electrospinning carbon fibers, which are expensive and low-throughput. In addition, pristine carbon nanotubes are chemically inert and highly hydrophobic, which makes/them difficult to be deposited on supports directly.

Natural plant cellulose can be processed to cellulose nanofibers (CNFs) [11]. As an emerging biomass resource, CNFs with aspect ratio up to 10^3 (4–20 nm in diameter) have been widely used in gas barrier film [12], functional papers [13], electrochemical electrode [14], and so on [15]. Therefore, it is advantageous to prepare carbon nanofiber with CNFs as the carbon precursor. In addition, CNFs can be obtained from natural plant cellulose by post treatment, including mechanical grinding and chemistry-assisted treatment. Among the methods of chemical-assisted nanofibrillation, TEMPO mediated oxidation can selectively oxidize the C6 primary hydroxyls of cellulose to produce high-density carboxylate on the CNFs surfaces [16,17]. These polar groups can provide abundant binding sites for metal sulfides.

Metal organic frameworks (MOFs), have been attracted widely

** Corresponding author.
* Corresponding author.
E-mail addresses: fengyi@njfu.edu.cn (Y. Feng), jfyao@njfu.edu.cn (J. Yao).

https://doi.org/10.1016/j.jallcom.2019.152911
0925-8388/© 2019 Elsevier B.V. All rights reserved.

for applications in gas separation and storage [18,19], catalysis [20], drug delivery [21], and energy storage [22–24] due to their well-defined structure and high surface areas. MOFs are formed by metal ions and organic linker through covalent coordination linkages and have showed great superiority as precursor preparing tailorable metal sulfides in energy application [25–28]. Among MOFs, zeolitic imidazolate frameworks (ZIFs) have been reported to synthesize unique nanomaterials as high-performance electrodes for Li-ion battery. For example, Wu et al. prepared symmetric porous Co_3O_4 hollow dodecahedra and $Zn_xCo_{3-x}O_4$ hollow polyhedra, which showed excellent electrochemical performance [29,30]. In addition, ultrafine ZnS nanorods rooting on carbon polyhedra was synthesized and exhibited superior performance [31]. Direct carbonization of MOFs can form carbon wrapped metal oxides or metal sulfides. However, the low conductivity is the major problem which limits their application.

Herein, Co_9S_8/carbonized CNFs (Co_9S_8/C-CNFs) have been synthesized by carbonization and sulfidation of CNFs/ZIF-67 composites. Carbonized CNFs act as conductive skeleton to connect carbonized ZIF-67 particles; facilitating the electron transfer and avoiding the agglomeration of particles. Meanwhile the carbonized organic linkers of ZIF-67 offers sufficient micropores and carbon layer to wrap Co_9S_8 nanoparticles, which can effectively limit the volume expansion of cobalt sulphides. Therefore, such Co_9S_8@C-CNFs with the above-mentioned unique structure is expected to show enhanced lithium ion storage and can be used as high-performance anode for LIBs.

2. Experimental

2.1. Materials

$Co(NO_3)_2 \cdot 6H_2O$ (≥98.5%), thioacetamide (99%) and ethanol were purchased from Sinopharm Chemical Reagent. 2-methylimidazole (Hmim) (≥98%) was purchased from Shanghai Aladdin. Cotton cellulose nanofibers (CNFs) suspension (1% w/v) was purchased from GuiLin QiHong Technology Co. Ltd.

2.2. Synthesis of ZIF-67/CNFs

The cotton cellulose nanofibers (CNFs) suspensions (1% w/v) (30 g) were firstly stirred vigorously. After dropwise addition of 5 mL $Co(NO_3)_2 \cdot 6H_2O$ (0.84 mol/L) in methanol without stirring, the suspensions aged 24 h for gelation. Then the resultant hydrogel was washed with methanol. 2.75 g Hmim was added into 20 mL methanol with stirring for 20 min the obtained hydrogel was immersed into Hmim solution for ZIF-67 growth for 24 h. Finally, the hydrogel was washed with methanol and exchanged the solvent to t-BuOH and freeze-drying.

2.3. Synthesis of Co_9S_8/C-CNFs

The obtained ZIF-67/CNFs was transferred to an alumina boat in a tube furnace for heating process with a heating rate 2 °C min^{-1} to 600 °C under a flowing Ar (30 mL min^{-1}) and tempered for 2 h. Then the black intermediate product was obtained and 0.1 g of the product and 0.3 g of thioacetamide were added into 40 mL ethanol with stirring for 20 min. The dispersion solution was transfer into Teflon-lined autoclave which was maintained at 180 °C for 24 h and cooled down naturally. The product was collected and washed with deionized water and ethanol, respectively.

2.4. Synthesis of ZIF-67

1 mmol of $Co(NO_3)_6 \cdot 6H_2O$ and 4 mmol of Hmim were dissolved in 25 mL methanol, respectively. Then Hmim solution immediately was added into cobalt nitrate solution with stirring and then aged for 24 h at room temperature. At last, the purple product was collected and washed with methanol three times and dried at 70 °C overnight.

2.5. Synthesis of Co_9S_8/C and carbonized C-CNFs

Co_9S_8/C was prepared similarly as above Co_9S_8/C-CNFs, except for using ZIF-67 instead of ZIF-67/CNFs as precursor. Carbonized CNFs (C-CNFs) was also prepared by carbonization and sulfidation method.

2.6. Material characterization

The XRD of samples was collected using Rigaku Smartlab with Cu Kα radiation (λ = 0.1542 nm) at 40 kV. SEM images were obtained using JSM-7600F (JEOL Ltd.,Japan). Raman spectra were collected using thermo with 532 nm laser excitation. Fourier transform infrared spectra (FT-IR) were characterized using the KBr wafer technique with Thermo Electron Nicolet-360 (USA). TEM image was collected by using JEOL JEM-2100 instrument at accelerating voltage of 200 kV. Thermal gravimetric analysis (TGA) was determined by a TA-60H (Shimadzu Corporation, Japan) under air atmosphere from 25 to 900 °C with a heating rate 5° min^{-1}.

2.7. Electrochemical measurements

The working electrode slurry was prepared by dispersing 70 wt% of active material, 20 wt% of Super-P and 10 wt% of polyvinylidene difluoride. The slurry was coated onto copper foil and dried in a vacuum oven at 80 °C overnight. The as-prepared electrode, Lithium foil as counter electrode, 1.0 M $LiPF_6$ in a 1:1 (v/v) mixture of ethyl carbonate/dimethyl carbonate as the electrolyte and Celgard 2500 as the separator were assembled into CR2016-type coin cell. The charge-discharge tests were conducted with a battery tester (LAND CT2001A). Cyclic voltammetry (CV) profiles and electrochemical impedance spectra (EIS) were performed with a CHI760e electrochemical workstation.

3. Results and discussion

Cellulose nanofibers were exposed to Co^{2+} solution to form homogeneous fibrous hydrogel (CNFs-Co^{2+}) through ionic gelation. When the organic linker (2-methylimidazole) was added into above system, ZIF-67 particles homogeneously grew on the CNFs. After calcination and sulfidation, the Co_9S_8/carbon nanofibers were synthesized (Scheme 1). The abundant carboxylate on the CNFs surface provides strong binding interactions and copious reaction sites for growth of ZIF-67. This strong binding between ZIF-67 and CNFs also maintains the close connection of 1D carbon fibers with metal sulfide after calcination and sulfidation.

XRD pattern of as prepared ZIF-67 agrees with the simulated pattern of ZIF-67 (Fig. 1a) [32]. CNFs show two broad diffraction peaks at around 15.7° and 22.3°, which are typical cellulose I crystalline structure [33]. XRD pattern of ZIF-67/CNFs indicates the presence of both ZIF-67 and CNFs. As shown in Fig. 1b, after calcination and sulfidation, the diffraction peaks of Co_9S_8/C (prepared by direct carbonization and sulfidation of ZIF-67) and Co_9S_8/C-CNFs at 29.8°, 31.2°, 52.0°, are ascribed to (331), (222) and (440) planes of cubic Co_9S_8 (JCPDS No. 65-6801). Some peaks such as (101), (102) and (110) planes are assigned to CoS (JCPDS No. 65-3418) in Co_9S_8/C, and this means that the cobalt chalcogenide is the mixture of Co_9S_8 and CoS. The peak of C (101) only exists in Co_9S_8/C but not Co_9S_8/C-CNFs, and this is perhaps because in the Co_9S_8/C-CNFs, the

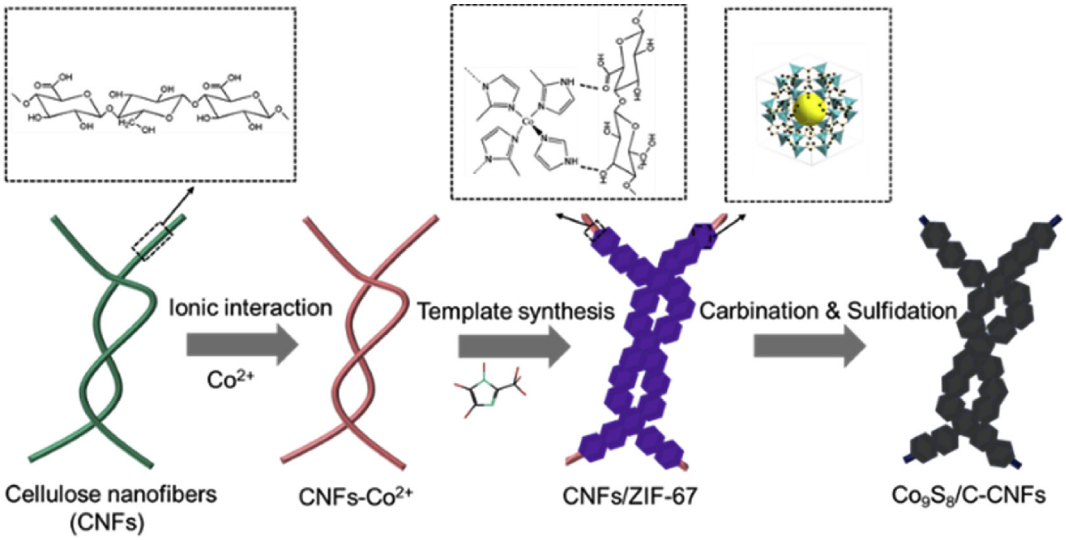

Scheme 1. Schematic illustration of the preparation of Co_9S_8/C-CNFs.

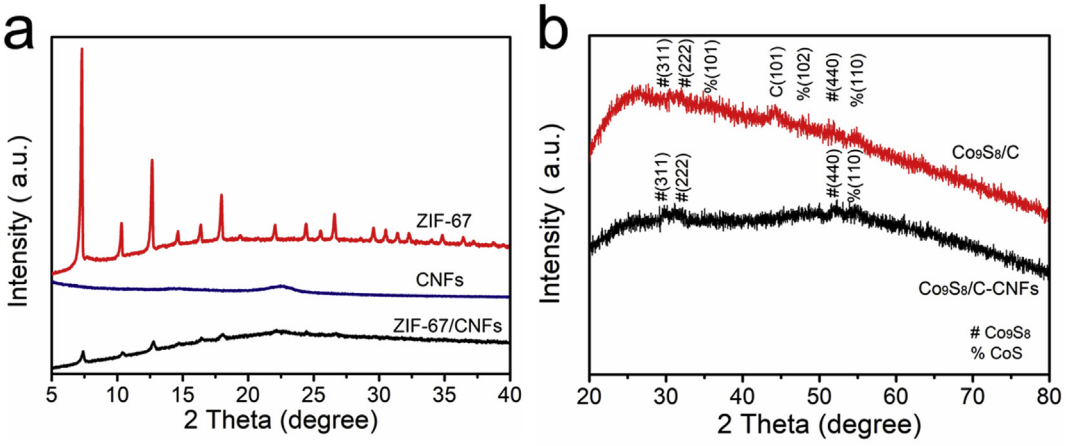

Fig. 1. XRD patterns of ZIF-67, ZIF-67/CNFs and CNFs (a); XRD patterns of Co_9S_8/C and Co_9S_8/C-CNFs-S (b).

carbon from CNFs covers carbon from ZIF-67, leading to the reduction of C (101) peak. However, the diffraction features of Co_9S_8 are greatly weakened due to cover of amorphous carbon.

The morphology of ZIF-67 and ZIF-67 after sulfidation observed using scanning electron microscopy (SEM) are showed in Fig. 2. The size of ZIF-67 crystal is about ~1 μm and particles are highly dispersed (Fig. 2a). In Fig. 2b, after calcination and sulfidation, ZIF-67 becomes shrunken with concave surfaces. Fig. 2c shows that ZIF-67 particles grow on the CNFs and form necklace-like structure, which interlaces to form complex network. Due to the close growth of ZIF-67 particles on CNFs, it is hard to find the CNFs. In addition, the size of ZIF-67 particles is ranged from 100 to 150 nm. In fact, the size of ZIF-67 grown on CNFs is smaller than that of pure ZIF-67 synthesized via normal method [34], because CNFs can favor ZIF-67 crystal nucleation over growth [35]. When the CNFs-Co^{2+} hydrogel was added into Hmim solution, the complex CNFs network provided sufficient attachment sites, which improve ZIF-67 nucleation on CNFs. The prepared method can effectively prevent the aggregation of ZIF-67 particles. After calcination and sulfidation, most of ZIF-67/CNFs can maintain size homogeneity and structural morphology of polyhedron cluster, but a small part of them was collapsed (Fig. 2d). Among ZIF-67/CNFs, CNFs convert to carbon fibers which connect Co_9S_8/carbon composites, providing stable channels for electron transport. In addition, CNFs have uniform sizes of 4–6 nm in width and about 1000 nm in length [36]. TEM image of Co_9S_8/C-CNFs clearly demonstrates the presence of carbonized-CNF that twined Co_9S_8/C particles (Fig. S1).

The chemistry structure of CNFs, ZIF-67/CNFs and ZIF-67 are analyzed by Fourier transform infrared spectroscopy (FT-IR) (Fig. 3a). After CNFs composited with ZIF-67, broad absorption located in 3428 cm^{-1} shifts to 3440 cm^{-1}, which derives from the stretching vibration of −OH groups of CNFs. In addition, the peak at 1622 cm^{-1} of CNFs is ascribed to the C=O stretching of carbonyl groups, which shifts to 1633 cm^{-1} after the CNFs hybridization with ZIF-67. These frequency variation of −OH and C=O bonding reflects the existence of hydrogen bonding between CNFs and ZIF-67. The strong interaction of CNFs and ZIF-67 can guarantee good connection of carbon fibers and Co_9S_8/carbon composites after the calcination and sulfidation.

The Raman spectra were used to further characterize Co_9S_8/C-CNFs and Co_9S_8/C, as presented in Fig. 3b. The two strong Raman peaks can be observed at 1320 and 1590 cm^{-1}, which correspond to sp^3-type disorder carbon form (D band) and sp^2-type graphited carbon form (G band), respectively. And the calculated I_D/I_G values

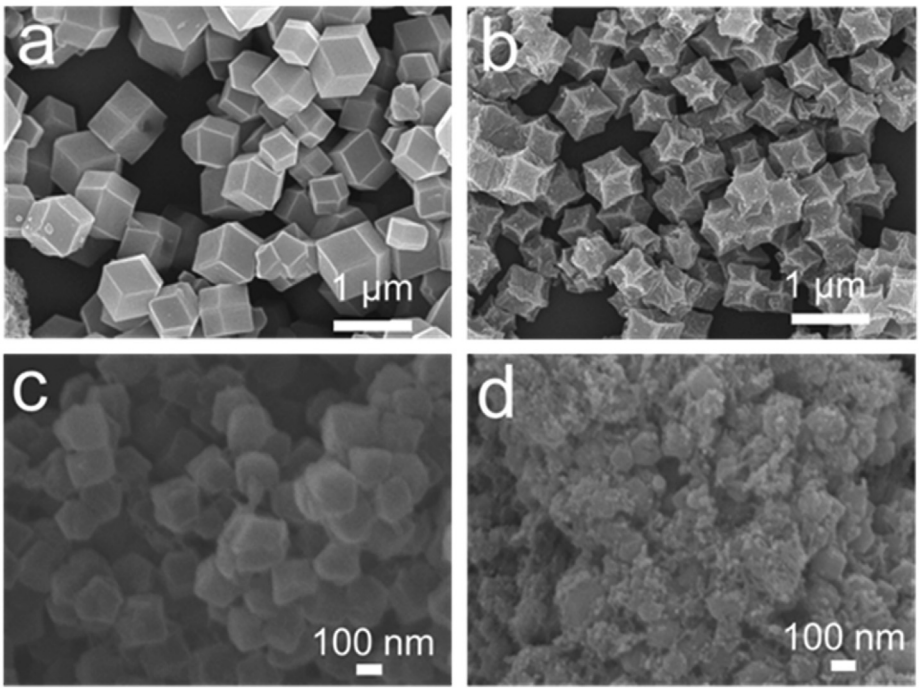

Fig. 2. SEM images of ZIF-67 (a), ZIF-67 after sulfidation (b), ZIF-67/CNFs (c) and ZIF-67/CNFs after sulfidation (d).

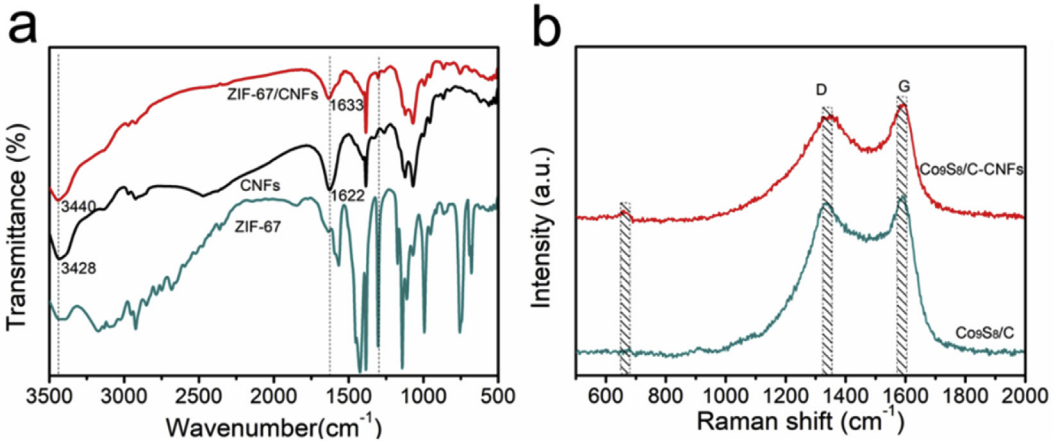

Fig. 3. FT-IR spectra of ZIF-67/CNFs, CNFs and ZIF-67 (a) and Raman spectra of Co_9S_8/C-CNFs and Co_9S_8/C (b).

of Co_9S_8/C-CNFs and Co_9S_8/C are 0.90 and 0.96, respectively, indicating Co_9S_8/C-CNFs has higher degree of graphitization than Co_9S_8/C. The incorporation of carbon nanofibers derived from CNFs can be beneficial to improve the degree of graphitization of the material and thus further increase the conductivity. In addition, there are the characteristic peaks below 1000 cm^{-1} which ascribed to vibration of S—Co bond in Co_9S_8 [37]. The amount of Co_9S_8 in Co_9S_8@C and Co_9S_8@C-CNFs can be roughly calculated by TGA (Fig. S2 in supporting information) [26], and the weight ratios of Co_9S_8 in composites are ca. 41 and 37 wt%, respectively.

To demonstrate their potential application, cyclic voltammetry (CV) test of Co_9S_8/C-CNFs as the anode material of LIBs was carried out (Fig. 4a), with potential range of 0.01—3 V at a scan rate of 0.1 mV s^{-1}. In the first discharge process, the cathodic peaks at 1.68 and 1.04 V could be ascribed to the process of Co_9S_8 being converted to $Li_xCo_9S_8$ and then transformed to Co. The cathodic peak at 0.60 V could be explained to the formation of solid electrolyte interface (SEI) film. The anodic peaks of first cycle at 1.33, 1.89, 2.33 V correspond to oxidation of above-mentioned products [38]. For the following two cycles, the cathodic peaks maintained at 1.33 and 0.67 V, and anodic peaks are centered at 1.36 and 1.9 V, reflecting good electrochemical reversibility.

The first three galvanostatic discharge/charge profiles of Co_9S_8/C-CNFs are measured at current density of 100 mA g^{-1} (Fig. 4b). In first discharge curve, there are two slope plateaus around 1.6 and 1.0 V, which are ascribed to formation of Co, corresponding to CV results. The initial discharge capacity was as high as 1545 mAh g^{-1} but it decreased significantly in the 2nd cycle resulting from the formation of SEI film and electrolyte decomposition. However, for the following cycles, the curves show a good overlap, indicating high reversibility of the charge/discharge process.

The cycling performance of Co_9S_8/C-CNFs was measured at 500 mA g^{-1}, together with that of Co_9S_8/C for comparison. In Fig. 4c, Co_9S_8/C-CNFs shows higher specific capacity than that of Co_9S_8/C,

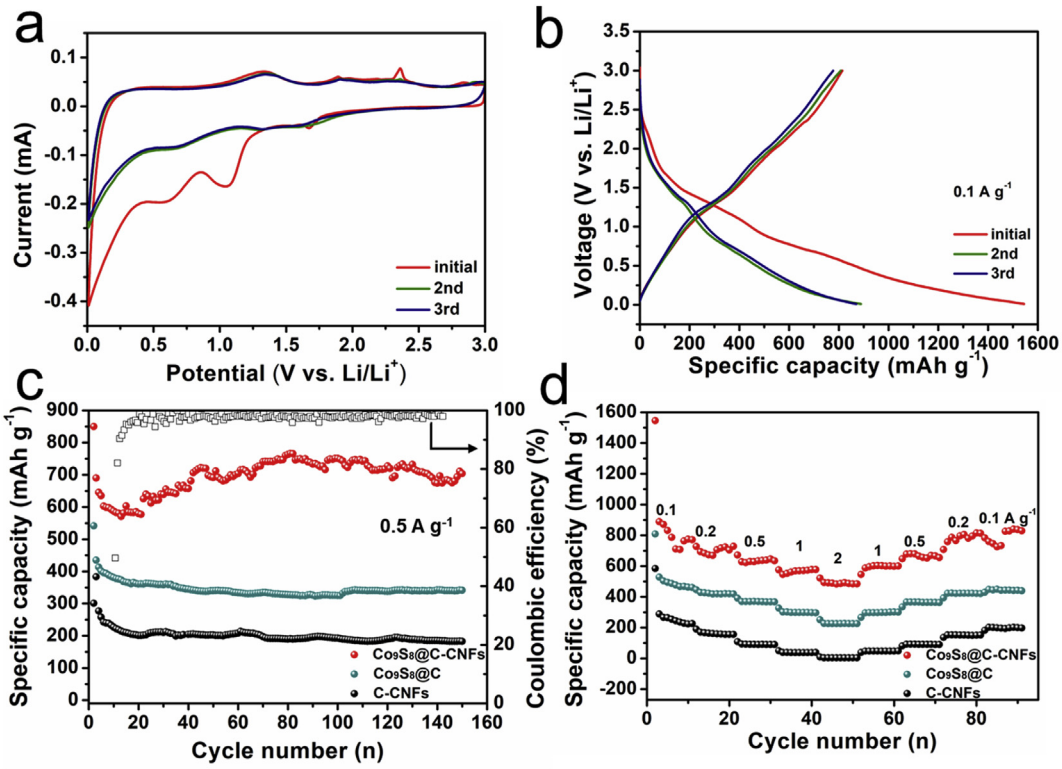

Fig. 4. CV profiles of the first three cycles at a scan rate of 0.1 mV s^{-1} (a) and charge-discharge curves of Co_9S_8/C-CNFs at a current density of 100 mA g^{-1}(b); cycling performance of Co_9S_8/C-CNFs, Co_9S_8/C and C-CNFs at a current density of 500 mA g^{-1} (c) and their rate performance (d).

suggesting the improved electrochemical performance. For Co_9S_8/C-CNFs, the specific capacity decreased firstly in the first 20 cycles and then increased, mainly due to the slow activation of active materials after several cycles of lithiation and delithiation. The specific capacity is 700 mAh g^{-1} after 150 cycles compared to that of 342 mAh g^{-1} for Co_9S_8/C. The improved lithium ion storage is mainly attributed to the unique pore structure of Co_9S_8/C-CNFs and improved conductivity resulting from carbonized CNFs. Fig. 4d shows that Co_9S_8/C-CNFs deliver a reversible discharge specific capacity of 772, 729, 634, 578, 484 mAh g^{-1} at 0.1, 0.2, 0.5, 1, 2 A g^{-1}, respectively. When current density was back to 1, 0.5, 0.2 and 0.1 A g^{-1}, the discharge specific capacities of 600, 656, 814, 830 mAh g^{-1} were resumed for Co_9S_8/C-CNFs, respectively, reflecting the superior cycling stability. By contrast, the Co_9S_8/C delivers much lower rate capacities of 460, 419, 367, 296, 225 mAh g^{-1} at 0.1, 0.2, 0.5, 1 and 2 A g^{-1} respectively. In addition, the carbonized CNFs were also measured and show a stable specific capacity of 183 mAh g^{-1} at 500 mA g^{-1} after 150 cycles, and the rate performance is stable. EIS measurements of Co_9S_8/C and Co_9S_8/C-CNFs (Fig. S3) conform that Co_9S_8/C-CNFs has lower charge-discharge resistance than that of Co_9S_8/C, further proving that the addition of CNFs benefits the lithium ion transport.

The growth of ZIF-67 particles on CNFs is beneficial to the improved electrochemical performance, mainly by the following contributions: a) CNFs functions as the support to avoid the agglomeration of ZIF-67 particles; b) CNFs greatly limit the growth of ZIF-67 particles; thus smaller ZIF-67 particles can be formed, and c) carbonized CNFs act as the conductive skeleton to facilitate the electron transfer. Therefore, compared to directly carbonization and sulfidation of ZIF-67 (Co_9S_8/C), ZIF-67/CNFs composites show superior advantages and the following Co_9S_8/C-CNFs exhibits significant improvement in lithium ion storage.

4. Conclusions

ZIF-67/CNFs were synthesized through in-situ growth of ZIF-67 on cellulose nanofibers, followed by calcination and sulfidation to form Co_9S_8/C-CNFs. The resulting product shows good electrochemical performance as anode material for LIBs: a high reversible specific capacity of 700 mAh g^{-1} at 500 mA g^{-1} after 150 cycles and a superior rate capability (772, 729, 634, 578, 484 mAh g^{-1} at current density of 0.1, 0.2, 0.5, 1, 2 A g^{-1}, respectively). The great improvement was ascribed to carbon nanofibers derived from cellulose nanofibers effectively connecting to Co_9S_8/carbon composites.

Declaration of competing interest

The authors declare that they have no known competing financial interests or personal relationships that could have appeared to influence the work reported in this paper.

Acknowledgements

This work was supported by the financial support of the Youth Fund of Natural Science Foundation of Jiangsu Province (BK20170919) and the National Natural Science Foundation of China (21808112), Jiangsu Province Six Talent Peaks Project (2016-XCL-043), and Priority Academic Program Development of Jiangsu Higher Education Institutions (PAPD).

Appendix A. Supplementary data

Supplementary data to this article can be found online at https://doi.org/10.1016/j.jallcom.2019.152911.

References

[1] J.B. Goodenough, K.-S. Park, The li-ion rechargeable battery: a perspective, J. Am. Chem. Soc. 135 (2013) 1167–1176, https://doi.org/10.1021/ja3091438.

[2] S. Guo, Y. Feng, W. Ding, X. Li, L. Yang, J. Yao, Design of porous Co_3O_4 nanosheets via one-step synthesis as high-performance anode materials for lithium-ion batteries, J. Solid State Electrochem. 23 (2019) 1–7, https://doi.org/10.1007/s10008-018-4101-1.

[3] X. Rui, H. Tan, Q. Yan, Nanostructured metal sulfides for energy storage, Nanoscale 6 (2014) 9889–9924, https://doi.org/10.1039/c4nr03057e.

[4] S. Guo, Y. Feng, J. Qiu, X. Li, J. Yao, Leaf-shaped bimetallic sulfides@ N-doped porous carbon as advanced lithium-ion battery anode, J. Alloy. Comp. 792 (2019) 8–15, https://doi.org/10.1016/j.jallcom.2019.03.398.

[5] R. Tian, Y. Zhou, H. Duan, Y. Guo, H. Li, K. Chen, D. Xue, H. Liu, MOF-derived hollow Co_3S_4 quasi-polyhedron/MWCNT nanocomposites as electrodes for advanced lithium ion batteries and supercapacitors, ACS Appl. Energy Mater. 1 (2018) 402–410, https://doi.org/10.1021/acsaem.7b00072.

[6] H. Wang, S. Lu, Y. Chen, L. Han, J. Zhou, X. Wu, W. Qin, Graphene/Co_9S_8 nanocomposite paper as a binder-free and free-standing anode for lithium-ion batteries, J. Mater. Chem. A 3 (2015) 23677–23683, https://doi.org/10.1039/C5TA06158J.

[7] Y. Liu, N. Zhang, L. Jiao, J. Chen, Tin nanodots encapsulated in porous nitrogen-doped carbon nanofibers as a free-standing anode for advanced sodium-ion batteries, Adv. Mater. 27 (2015) 6702–6707, https://doi.org/10.1002/adma.201503015.

[8] S.J. Cho, K.H. Choi, J.T. Yoo, J.H. Kim, Y.H. Lee, S.J. Chun, S.B. Park, D.H. Choi, Q. Wu, S.Y. Lee, Hetero-nanonet rechargeable paper batteries: toward ultrahigh energy density and origami foldability, Adv. Funct. Mater. 25 (2015) 6029–6040, https://doi.org/10.1002/adfm.201502833.

[9] H. Wang, Z. Chen, Y. Liu, H. Xu, L. Cao, H. Qing, R. Wu, Hierarchically porous-structured $Zn_xCo_{1-x}S$@C-CNT nanocomposites with high-rate cycling performance for lithium-ion batteries, J. Mater. Chem. A 5 (2017) 23221–23227, https://doi.org/10.1039/c7ta07993a.

[10] L. Fei, B.P. Williams, S.H. Yoo, J.M. Carlin, Y.L. Joo, A general approach to fabricate free-standing metal sulfide@carbon nanofiber networks as lithium ion battery anodes, Chem. Commun. 52 (2016) 1501–1504, https://doi.org/10.1039/c5cc06957b.

[11] R.J. Moon, A. Martini, J. Nairn, J. Simonsen, J. Youngblood, Cellulose nanomaterials review: structure, properties and nanocomposites, Chem. Soc. Rev. 40 (2011) 3941–3994, https://doi.org/10.1039/C0CS00108B.

[12] H. Fukuzumi, T. Saito, T. Iwata, Y. Kumamoto, A. Isogai, Transparent and high gas barrier films of cellulose nanofibers prepared by TEMPO-mediated oxidation, Biomacromolecules 10 (2008) 162–165, https://doi.org/10.1021/bm801065u.

[13] H. Koga, T. Saito, T. Kitaoka, M. Nogi, K. Suganuma, A. Isogai, Transparent, conductive, and printable composites consisting of TEMPO-oxidized nanocellulose and carbon nanotube, Biomacromolecules 14 (2013) 1160–1165, https://doi.org/10.1021/bm400075f.

[14] Y. Kuang, C. Chen, G. Pastel, Y. Li, J. Song, R. Mi, W. Kong, B. Liu, Y. Jiang, K. Yang, L. Hu, Conductive cellulose nanofiber enabled thick electrode for compact and flexible energy storage devices, Adv. Energy. Mater. 8 (2018) 1302898–1302906, https://doi.org/10.1002/aenm.201802398.

[15] X.-F. Zhang, Y. Feng, Z. Wang, M. Jia, J. Yao, Fabrication of cellulose nanofibrils/UiO-66-NH_2 composite membrane for CO_2/N_2 separation, J. Membr. Sci. 568 (2018) 10–16, https://doi.org/10.1016/j.memsci.2018.09.055.

[16] A. Isogai, T. Saito, H. Fukuzumi, TEMPO-oxidized cellulose nanofibers, Nanoscale 3 (2011) 71–85, https://doi.org/10.1039/C0NR00583E.

[17] T. Saito, S. Kimura, Y. Nishiyama, A. Isogai, Cellulose nanofibers prepared by TEMPO-mediated oxidation of native cellulose, Biomacromolecules 8 (2007) 2485–2491, https://doi.org/10.1021/bm0703970.

[18] R. Banerjee, H. Furukawa, D. Britt, C. Knobler, M. O'Keeffe, O.M. Yaghi, Control of pore size and functionality in isoreticular zeolitic imidazolate frameworks and their carbon dioxide selective capture properties, J. Am. Chem. Soc. 131 (2009) 3875–3877, https://doi.org/10.1021/ja809459e.

[19] E. Jeong, W.R. Lee, D.W. Ryu, Y. Kim, W.J. Phang, E.K. Koh, C.S. Hong, Reversible structural transformation and selective gas adsorption in a unique aqua-bridged Mn (II) metal-organic framework, Chem. Commun. 49 (2013) 2329–2331, https://doi.org/10.1039/C3CC00093A.

[20] R.-Q. Zou, H. Sakurai, S. Han, R.-Q. Zhong, Q. Xu, Probing the lewis acid sites and CO catalytic oxidation activity of the porous metal-organic polymer [Cu (5-methylisophthalate)], J. Am. Chem. Soc. 129 (2007) 8402–8403, https://doi.org/10.1021/ja071662s.

[21] P. Horcajada, T. Chalati, C. Serre, B. Gillet, C. Sebrie, T. Baati, J.F. Eubank, D. Heurtaux, P. Clayette, C. Kreuz, Porous metal-organic-framework nanoscale carriers as a potential platform for drug delivery and imaging, Nat. Mater. 9 (2010) 172, https://doi.org/10.1038/nmat2608.

[22] T. Wang, Z. Kou, S. Mu, J. Liu, D. He, I.S. Amiinu, W. Meng, K. Zhou, Z. Luo, S. Chaemchuen, F. Verpoort, 2D dual-metal zeolitic-imidazolate-framework-(ZIF)-derived bifunctional air electrodes with ultrahigh electrochemical properties for rechargeable zinc-air batteries, Adv. Funct. Mater. 28 (2018) 1705048, https://doi.org/10.1002/adfm.201705048.

[23] Y.M. Chen, L. Yu, X.W. Lou, Hierarchical tubular structures composed of Co_3O_4 hollow nanoparticles and carbon nanotubes for lithium storage, Angew. Chem. Int. Ed. 55 (2016) 5990–5993, https://doi.org/10.1002/anie.201600133.

[24] Z. Chen, R. Wu, H. Wang, K.H. Zhang, Y. Song, F. Wu, F. Fang, D. Sun, Embedding ZnSe nanodots in nitrogen-doped hollow carbon architectures for superior lithium storage, Nano. Res. 11 (2018) 966–978, https://doi.org/10.1007/s12274-017-1709-x.

[25] J. Zhang, L. Yu, X.W. Lou, Embedding CoS_2 nanoparticles in N-doped carbon nanotube hollow frameworks for enhanced lithium storage properties, Nano. Res. 10 (2017) 4298–4304, https://doi.org/10.1007/s12274-016-1394-1.

[26] Z. Chen, R. Wu, M. Liu, H. Wang, H. Xu, Y. Guo, Y. Song, F. Fang, X. Yu, D. Sun, General synthesis of dual carbon-confined metal sulfides quantum dots toward high-performance anodes for sodium-ion batteries, Adv. Funct. Mater. 27 (2017), https://doi.org/10.1002/adfm.201702046, 1702046.

[27] R. Wu, D.P. Wang, X. Rui, B. Liu, K. Zhou, A.W. Law, Q. Yan, J. Wei, Z. Chen, In-situ formation of hollow hybrids composed of cobalt sulfides embedded within porous carbon polyhedra/carbon nanotubes for high-performance lithium-ion batteries, Adv. Mater. 27 (2015) 3038–3044, https://doi.org/10.1002/adma.201500783.

[28] Y. Liu, Z. Chen, H. Jia, H. Xu, M. Liu, R. Wu, Iron-doping-induced phase transformation in dual-carbon-confined cobalt diselenide enabling superior lithium storage, ACS Nano (2019), https://doi.org/10.1021/acsnano.9b02928.

[29] R. Wu, X. Qian, X. Rui, H. Liu, B. Yadian, K. Zhou, J. Wei, Q. Yan, X.Q. Feng, Y. Long, Zeolitic imidazolate framework 67-derived high symmetric porous Co_3O_4 hollow dodecahedra with highly enhanced lithium storage capability, Small 10 (2014) 1932–1938, https://doi.org/10.1002/smll.201303520.

[30] R. Wu, X. Qian, K. Zhou, J. Wei, J. Lou, P.M. Ajayan, Porous spinel $Zn_xCo_{3-x}O_4$ hollow polyhedra templated for high-rate lithium-ion batteries, ACS Nano 8 (2014) 6297–6303, https://doi.org/10.1021/nn501783n.

[31] Z. Chen, R. Wu, H. Wang, Y. Jiang, L. Jin, Y. Guo, Y. Song, F. Fang, D. Sun, Construction of hybrid hollow architectures by in-situ rooting ultrafine ZnS nanorods within porous carbon polyhedra for enhanced lithium storage properties, Chem. Eng. J. 326 (2017) 680–690, https://doi.org/10.1016/j.cej.2017.06.009.

[32] Z. Jiang, Z. Li, Z. Qin, H. Sun, X. Jiao, D. Chen, LDH nanocages synthesized with MOF templates and their high performance as supercapacitors, Nanoscale 5 (2013) 11770–11775, https://doi.org/10.1039/C3NR03829G.

[33] J. You, J. Cao, Y. Zhao, L. Zhang, J. Zhou, Y. Chen, Improved mechanical properties and sustained release behavior of cationic cellulose nanocrystals reinforced cationic cellulose injectable hydrogels, Biomacromolecules 17 (2016) 2839–2848, https://doi.org/10.1021/acs.biomac.6b00646.

[34] J. Shao, Z. Wan, H. Liu, H. Zheng, T. Gao, M. Shen, Q. Qu, H. Zheng, Metal organic frameworks-derived Co_3O_4 hollow dodecahedrons with controllable interiors as outstanding anodes for Li storage, J. Mater. Chem. A 2 (2014) 12194–12200, https://doi.org/10.1039/C4TA01966K.

[35] L. Zhu, L. Zong, X. Wu, M. Li, H. Wang, J. You, C. Li, Shapeable fibrous aerogels of metal-organic-frameworks templated with nanocellulose for rapid and large-capacity adsorption, ACS Nano 12 (2018) 4462–4468, https://doi.org/10.1021/acsnano.8b00566.

[36] X.-F. Zhang, Y. Feng, C. Huang, Y. Pan, J. Yao, Temperature-induced formation of cellulose nanofiber film with remarkably high gas separation performance, Cellulose 24 (2017) 5649–5656, https://doi.org/10.1007/s10570-017-1529-x.

[37] X. Hu, J. Jia, G. Wang, J. Chen, H. Zhan, Z. Wen, Reliable and general route to inverse opal structured nanohybrids of carbon-confined transition metal sulfides quantum dots for high-performance sodium storage, Adv. Energy. Mater. 8 (2018), https://doi.org/10.1002/aenm.201801452.

[38] W. Shi, J. Zhu, X. Rui, X. Cao, C. Chen, H. Zhang, H.H. Hng, Q. Yan, Controlled synthesis of carbon-coated cobalt sulfide nanostructures in oil phase with enhanced Li storage performances, ACS Appl. Mater. Interfaces 4 (2012) 2999–3006, https://doi.org/10.1021/am3003654.